Ceramics International 49 (2023) 16732–16739

Contents lists available at ScienceDirect

Ceramics International

journal homepage: www.elsevier.com/locate/ceramint

A new green procedure to obtain and photosensitize SnO_2, in one step, for solar photocatalysis using natural dyes

Estefania Silva [a], Clemente G. Alvarado-Beltrán [a,**], Alberto Gaxiola [a], Víctor M. Orozco-Carmona [b], Priscy Alfredo Luque [c], Andrés Castro-Beltrán [a,*]

[a] Universidad Autónoma de Sinaloa, Fuente de Poseidón y Prol. Ángel Flores S/N, C.P. 81223, Los Mochis, Sinaloa, Mexico
[b] Centro de Investigación en Materiales Avanzados, S.C, Ave. Miguel de Cervantes 120, Complejo Industrial Chihuahua, C.P. 31109, Chihuahua, Chihuahua, Mexico
[c] Universidad Autónoma de Baja California, Carretera Transpeninsular Ensenada-Tijuana 3917, Colonia Playitas, C.P. 22860, Ensenada, Baja California, Mexico

ARTICLE INFO

Handling Editor: Dr P. Vincenzini

Keywords:
Green synthesis
Tin oxide
Photosensitization
Natural dye
Anthocyanin

ABSTRACT

In recent years, the synthesis of tin oxide (SnO_2) nanoparticles (NPs) through green methods has gained attention due to their potential application in photocatalysis. However, as SnO_2 can only be activated by UV radiation, developing new photocatalysts with high performance under solar light is a fundamental goal of many researchers. This paper proposes a one-step sustainable procedure to simultaneously synthesize and photosensitize SnO_2 NPs using natural dyes, ensuring a good performance under solar radiation. Characterization through TGA, FTIR, UV–vis, XRD, and TEM confirms the effect of the extracts on the one-step synthesis and photosensitization of the NPs. Finally, the photocatalytic activity of the photosensitized SnO_2 showed a significant improvement in comparison to unsensitized SnO_2, i.e., while unsensitized SnO_2 degraded 11% of an organic pollutant, the sensitized SnO_2 achieved up to 97% degradation after 120 min of exposure to sunlight.

1. Introduction

Semiconductor photocatalysis is a versatile procedure applied in diverse fields such as water splitting, energy generation, and degradation of pollutants [1]. Particularly, the degradation of pollutants stands out because water has become an increasingly scarce resource as a consequence of waste produced by human activities. One of the primary sources of water contamination is textile production. This industry is responsible for discharging significant amounts of chemical waste (heavy metals, synthetic dyes, etc.) to waterbodies [2,3]. In this sense, synthetic organic dyes contribute to water contamination and make it unfit for drinking or other uses [3]. Therefore, removing synthetic dyes from wastewater is essential due to their complex structure and low biodegradability [4].

Although there are plenty of methods for water treatment, photocatalysis is a competitive alternative for the elimination of synthetic dyes due to its simplicity, low toxicity, and high efficiency [5,6]. Many semiconductors have been used as photocatalysts in recent years, mainly metal oxides and carbon-based nanomaterials, both with particular benefits [7–9]. However, metal oxide semiconductors are especially abundant, low cost, chemically stable, and show good photocatalytic activity to degrade various environmental pollutants [10,11]. In this sense, besides the general virtues of metal oxide semiconductors, SnO_2 is not toxic, has low resistivity, good thermal stability, and high optical transmittance [12].

On the other hand, due to its wide bandgap (3.4 eV) [13], SnO_2 can only be activated under UV irradiation. However, the sunlight that reaches the earth's surface is constituted by about 45% of visible light (λ = 400–700 nm), while UV light (λ < 387 nm) represents less than 5% and, therefore, the solar photocatalytic activity of SnO_2 is limited [14,15].

Different approaches have been proposed to improve the solar photocatalytic activity of SnO_2, such as doping [16], the formation of nanocomposite materials [17–19], selective morphology [20], surface ion modification [21,22], or photosensitization by dyes (either synthetic or natural) [23,24]. Photosensitization causes the dye molecules to broaden the range of wavelengths that SnO_2 can absorb, and as a consequence, the performance of the material under sunlight improves [25].

Currently, natural dyes have become a sustainable alternative to

* Corresponding author.
** Corresponding author.
E-mail addresses: calvarado@uas.edu.mx (C.G. Alvarado-Beltrán), andres.castro@uas.edu.mx (A. Castro-Beltrán).

https://doi.org/10.1016/j.ceramint.2023.02.034
Received 17 November 2022; Received in revised form 12 January 2023; Accepted 6 February 2023
Available online 15 February 2023

synthetic ones due to their low cost, accessibility, non-toxicity, biodegradability, and a broad range of absorption [26–28]. There are plenty of natural dyes that are able to absorb visible light, such as anthocyanins, betalains, carotenes, and chlorophylls [29–31]. Among these, anthocyanins and betalains have been often used as photosensitizers in photovoltaic [32,33] and photocatalytic applications [34].

In the literature, the impregnation method has been used to photosensitize semiconductor materials, i.e., the dye is added after the synthesis in a later step [35,36]. On the other hand, because the same natural extracts have been used for both the synthesis and photosensitization of metal oxides, green synthesis emerges as a plausible alternative to carry out these processes in a single step and, this way, develop a significantly more efficient procedure [37–39].

It has been reported that plant biomolecules such as phenolic acids, flavonoids, polysaccharides, and terpenoids, among others, can act as reducing and stabilizing agents to assist in the production of nanoparticles [40].

In the Americas, plants such as *Vaccinium corymbosum* (blueberry), *Rubus glaucus* (blackberry), and *Beta vulgaris* (beetroot), are prolific, and their active components can be used as sensitizers in semiconductors for photocatalytic applications.

In this sense, *Vaccinium corymbosum* is a perennial flowering plant with blue-colored berries. The extracts of this fruit contain diverse anthocyanins and other phenolic compounds [41]. On the other hand, *Rubus* glaucus is a dark red berry mainly used to manufacture jams, juices, and wine. Its extracts contain a great variety of active compounds, but the most abundant are tannins and anthocyanins (mostly cyanidin) [42]. *Beta vulgaris* is a root, commonly eaten in salads, drunk in juices, and used as a food dye. Betalain is the compound that colors beet crimson and presents characteristics very similar to anthocyanins. The extracts of these plants have been studied mainly with two approaches, i.e., as a photosensitizer in solar cells [43–45] and as reducing agents in the green synthesis of semiconductor oxides [37,39,46].

This study presents a novel green approach to simultaneously synthesize and photosensitize SnO_2 nanoparticles. This results in a more efficient and environmentally friendly method to produce SnO_2 nanoparticles with an excellent solar photocatalytic activity using natural dye extracts.

2. Material and methods

2.1. Materials

The reagents used were stannous chloride ($SnCl_2$, FagaLab) as the precursor for Sn, acetic acid (CH_3COOH) as a catalyst, and locally purchased vegetables (blackberry, blueberry, and beetroot). On the other hand, methylene blue (FagaLab) was used as a model organic pollutant for the photocatalytic tests.

2.2. Extraction of the natural dyes

Three different fruits containing anthocyanins (blackberry and blueberry) and betalains (beetroot) were used to obtain natural dye extracts. All of them were thoroughly washed with water prior to use. To obtain the blueberry extract, the fresh fruit was placed in a dehydrator for 20 h at 65 °C. Subsequently, 10 g of the dehydrated fruit was weighed, cut into small pieces, and mixed with 100 ml of deionized water. Later, this mixture was heated to 90 °C for 2 h. For blackberry, 100 g of the fresh fruit was weighed, halved, added to 100 ml of deionized water, and then heated to 90 °C for 60 min. Beetroots were cut into small pieces and then processed in a juicer. All the extracts obtained were centrifuged to remove the solids and then stored in a refrigerator at 4 °C for later use.

2.3. Synthesis of SnO_2 nanoparticles

Pure SnO_2 nanoparticles were synthesized through the hydrothermal method as a comparison blank. First, 3.35 g of tin chloride ($SnCl_2$) were dissolved in 25.4 ml of deionized water under constant stirring for 20 min. Later, 3.39 ml of acetic acid (CH_3COOH) were added to the mixture, keeping agitation until a homogeneous solution was obtained (for approximately 30 min). Next, this solution was poured into a 50 ml autoclave and then and then heated in an oven to 200 °C for 6 h. Afterward, the precipitate was collected, washed with deionized water, centrifuged, and dried at room temperature. Finally, the material was pulverized with a mortar and stored.

2.4. Green synthesis of SnO_2 nanoparticles

For the green synthesis of SnO_2 nanoparticles, 40 mL of plant extract (see Table 1) was mixed with 2 g of tin chloride ($SnCl_2$) in a beaker. The mixture was then heated to 60 °C and maintained under constant stirring for 4 h. Later, the mixture was allowed to cool at room temperature and washed with abundant water using three cycles of centrifugation of 10 min each at 6000 rpm. After washing, the samples were placed in a Petri dish and dried at room temperature. Finally, the samples were pulverized with a mortar until a fine powder was obtained.

2.5. Characterization

The materials' optical properties and bandgap energy were studied using ultraviolet–visible (UV–Vis) spectroscopy using a Lambda 365 PerkinElmer spectrophotometer. A 200–800 nm wavelength range, a collection width of 2 nm, and a scan speed of 480 nm/min were used. The morphological studies of the nanoparticles were performed using transmission electron microscopy (TEM) images of the particles obtained through a JEM-2100 Transmission Electron Microscope, using a LaB6 filament, operated at a voltage of 200 kV. The structure and crystalline phases of the samples obtained were characterized by X-ray diffraction (XRD) in a Panalytical X-Pertsystem diffractometer, using Cu Kα radiation at 40 kV and 35 mA, with a 2θ scanning angle variation between 10° and 80°. Further analysis to examine the nanoparticles formation associated with the extract infrared spectra were carried out on a Bruker Alpha FTIR spectrophotometer. Samples were analyzed in transmittance mode using KBr pellets as a blank. The spectra were acquired as the average of 16 scans with a resolution of 4 cm^{-1} in the range of 4000–500 cm^{-1}. The methylene blue (MB) absorbance was measured through UV–visible spectroscopy using a Shimadzu 1800 spectrophotometer.

2.6. Photocatalytic activity

SnO_2 nanoparticles were used to study MB degradation under solar radiation. The study consisted of adding 50 mg of nanoparticles in 50 ml of MB solution at 15 mg/L (15 ppm) to achieve a ratio of 1:1 mg/ml. This solution was stirred in the dark for 30 min until adsorption-desorption equilibrium was reached. Afterward, the solutions were exposed to sunlight for 2 h. The experiment was carried out on February 26th, 2020, in Los Mochis, Mexico, from 11:00 a.m. to 1:00 p.m. During this time, 2 mL samples were collected every 20 min, and the MB concentration was analyzed via UV–vis spectroscopy. This procedure was followed for all the obtained samples.

Table 1
Dosage of the solutions used for the synthesis of the SnO_2 nanoparticles.

Extract	Sample ID	Prepared extract	DI water	Total volume
Beetroot	SnO_2-beetroot	40 ml	0 ml	40 ml
Blackberry	SnO_2-blackberry	30 ml	10 ml	
Blueberry	SnO_2-blueberry	30 ml	10 ml	

3. Results and discussion

3.1. Characterization of SnO_2 nanoparticles

Fig. 1a shows the FTIR spectra for pure SnO_2 nanoparticles obtained through the hydrothermal method (SnO_2), and through green synthesis (SnO_2-blackberry, SnO_2-blueberry, and SnO_2-beetroot). The FTIR spectra for SnO_2 shows two bands. The first one at around 3377 cm^{-1} is attributed to the stretching vibrations of OH bonds characteristic of water molecules adsorbed on the material's surface. The second one can be observed at about 500 cm^{-1}, attributed to the vibrations of the Sn–O–Sn bond characteristic of SnO_2 [47]. As shown in Fig. 1a, SnO_2-blackberry, SnO_2-blueberry, and SnO_2-beetroot exhibit the band at around 500 cm^{-1} attributed to Sn–O–Sn bond vibrations, which confirms the presence of SnO_2. Additionally, the bands observed at 2932 cm^{-1}, 1724 cm^{-1}, 1015 cm^{-1}, and 1058 cm^{-1} are attributed to the aromatic rings and functional groups of anthocyanins present in blackberry and blueberry extracts [48]. In contrast, the bands at around 2917 cm^{-1}, 1638 cm^{-1}, 1060 cm^{-1}, 1016 cm^{-1}, and 1123 cm^{-1} observed in the SnO_2-beetroot spectrum correspond to the functional groups of betalain molecules, which are in accordance with the literature [39]. These results indicate that SnO_2 was successfully synthesized and functionalized with the extracts.

Fig. 1b shows the thermogravimetric analysis for SnO_2, SnO_2-blackberry, SnO_2-blueberry, and SnO_2-beetroot. The SnO_2 thermogram displays a slight weight loss (~1.87%) in the 25 °C–700 °C range, similar to reported literature [49]. In addition, two other losses can be observed in the SnO_2-blackberry, SnO_2-blueberry, and SnO_2-beetroot thermograms. The first weight loss (~6%) appears around 100 °C and is associated with the evaporation of surface adsorbed water molecules. The second weight loss (~30%) is observed in the 250 °C–500 °C range and it is attributed to the decomposition of organic molecules (flavonoids, anthocyanins, betalains, tannins, glucose. etc.) used during the green synthesis of the material [50]. These results suggest there are extract molecules in the obtained material, which indicates there has been a functionalization of the SnO_2 during the green synthesis.

The XRD patterns for SnO_2, SnO_2-blackberry, SnO_2-blueberry, and SnO_2-beetroot are shown in Fig. 1c. The XRD pattern for SnO_2 shows a series of well-defined peaks at 26.4°, 33.7°, 37.7°, 51.8°, 54.8°, 61.8°, 65.9°, 71.0°, and 78.3°, which can be indexed to the (110), (101), (200), (211), (220), (310), (301), (202) and (222) crystalline planes, respectively. These planes correspond to rutile phase SnO_2 (JCPDS No. 41–1445, tetragonal), with no secondary phases [51]. On the other hand, SnO_2-blackberry, SnO_2-blueberry, and SnO_2-beetroot XRD patterns show only two broad peaks at 28.6° and 51.9°, associated to (110) and (211) planes of SnO_2 in rutile phase. The absence of sharp defined peaks can be attributed to the organic molecules from the extract (see Fig. 1a and b) surrounding the material, affecting the SnO_2 nanoparticles structural arrangement, which prevented the diffraction [52].

Fig. 1d shows the UV–Vis spectra of SnO_2, SnO_2-blackberry, SnO_2-blueberry, and SnO_2-beetroot. In the UV–vis spectra for SnO_2, a single absorption band is observed in the UV region around 286 nm, this band is characteristic of SnO_2 transitions [53]. On the other hand, two bands are observed for UV–vis spectra of SnO_2-beetroot, SnO_2-blackberry, and SnO_2-blueberry. The first absorption band located in the UV region around 286 nm, which is attributed to the transitions of SnO_2. In the second absorption band varies from 517 nm, 562 nm y 580 nm, respectively. This result is attributed to the SnO_2 modified with anthocyanins and betalains present in the extracts [54,55]. These results confirm the synthesis and functionalization of SnO_2 using different extracts.

Fig. 2 shows the bandgap values calculated from the UV–vis spectra using the Tauc model [56] for the SnO_2, SnO_2-blueberry, SnO_2-blackberry, and SnO_2-beetroot samples. For SnO_2 (Fig. 2a), the bandgap was ~3.0 eV, agreeing with the literature for the SnO_2 obtained by the hydrothermal method [57]. The bandgap values calculated for the SnO_2-blueberry, SnO_2-blackberry, and SnO_2-beetroot (Fig. 2b–d), were 2.14, 2.21, and 2.4 eV, respectively. These results show a reduction of the bandgap in comparison to the SnO_2, which can be attributed to the photosensitizer effect of the extracts [25,58].

Fig. 3 shows the morphologies of the SnO_2, SnO_2-blackberry, SnO_2-blueberry, and SnO_2-beetroot samples obtained by transmission electron

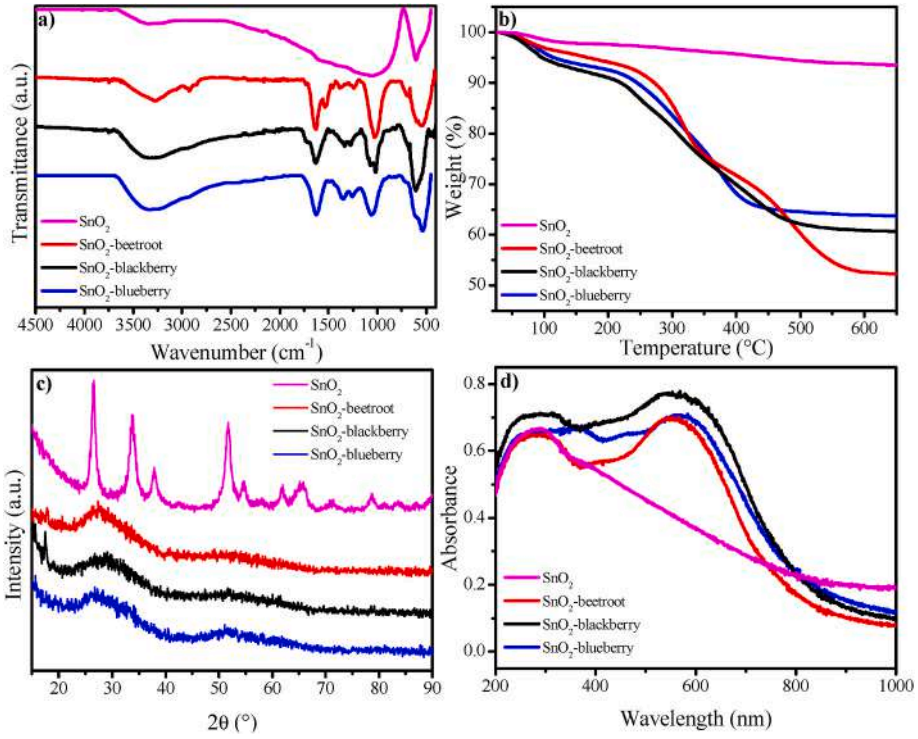

Fig. 1. FTIR spectra (a), thermogravimetric analysis (b), X-ray diffraction patterns (c), and UV–vis absorption spectra (d) for the prepared SnO_2 nanoparticles.

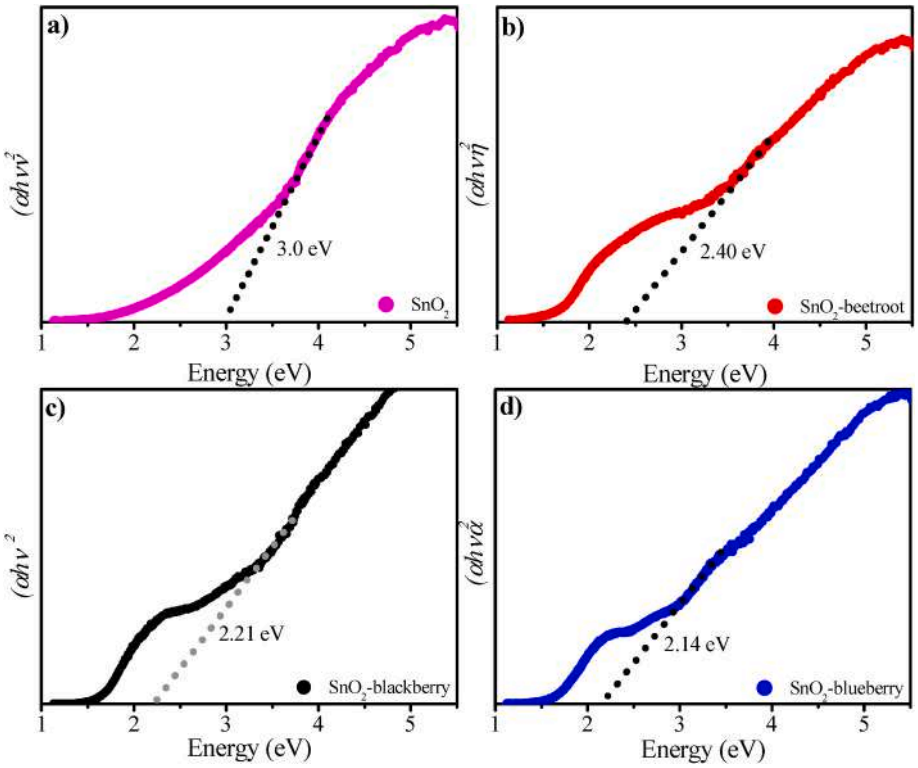

Fig. 2. Tauc plot and band gap values for SnO_2 (a), SnO_2-beetroot (b), SnO_2-blackberry (c), and SnO_2-blueberry (d) samples.

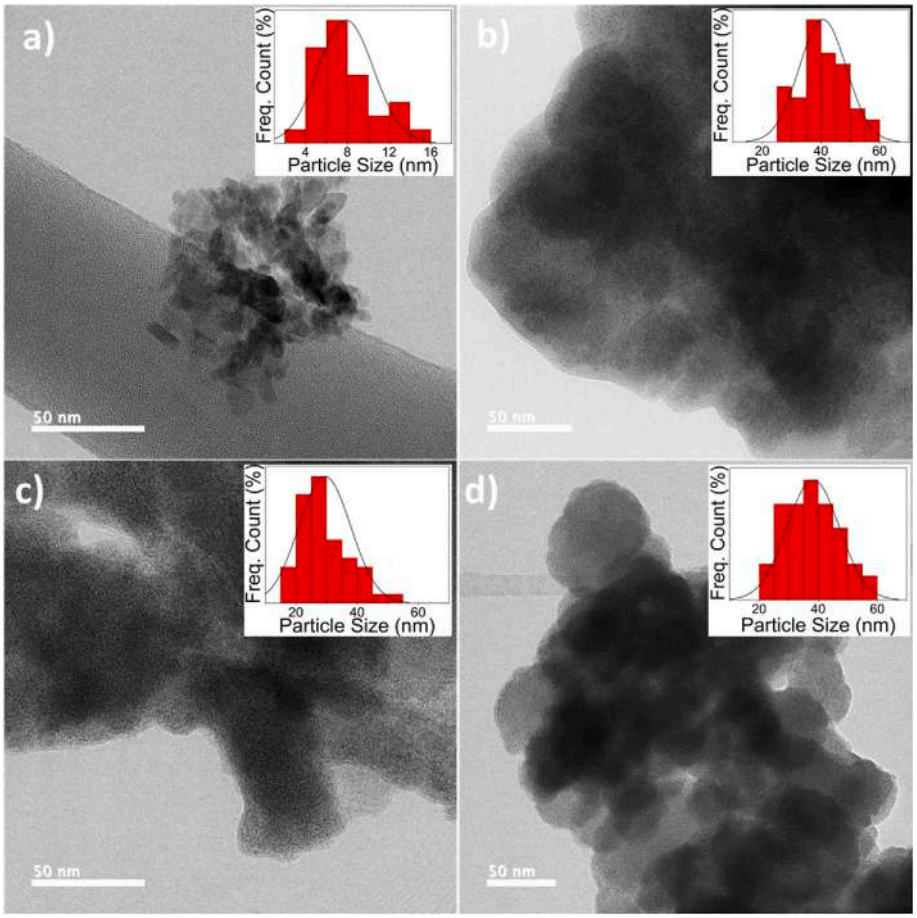

Fig. 3. Particle size distribution and TEM micrographs of SnO_2 (a), SnO_2-beetroot (b) SnO_2-blackberry and SnO_2-blueberry (d).

microscopy (TEM) analysis. In the pure SnO_2 sample (Fig. 3a), we can observe the presence of agglomerated nanoparticles with a quasi-spherical morphology and an average size of 7.87 nm. These results are consistent with those reported in literature [8]. Meanwhile, for the SnO_2-blackberry, SnO_2-blueberry, and SnO_2-beetroot samples (Fig. 5b–d) the presence of agglomerated nanoparticles with spherical morphology and an average size around of 29.51 nm, 38.35 nm, and 40.18 nm, respectively, is observed. The size increase compared to the SnO_2 sample can be attributed to the extract, which acts as a chelating and stabilizing agent, causing the size increase and agglomeration of the SnO_2 nanoparticles [51].

Fig. 4 shows the HRTEM images and electron diffraction patterns (SAED) of the selected area of the SnO_2 nanoparticles. The SnO_2 micrograph (Fig. 4a) clearly shows the presence of several crystallographic planes with interplanar distances around 0.27 nm and 0.33 nm (Fig. 4b). Moreover, they correspond to planes 110 and 101, characteristic of SnO_2 nanoparticles [52]. Furthermore, the SAED results (Fig. 4c) show a pattern of sharp dots and rings corresponding to planes (101), (110), (200), (211), and (310), which are characteristic of SnO_2 in its rutile phase according to JCPDS card 41–1445, confirming it has been successfully obtained [16]. It is worth mentioning that these results are consistent with what was observed in the XRD pattern (see Fig. 1c). The results are similar to those mentioned above for the SnO_2-beetroot micrograph (Fig. 4d–e). The crystallographic planes are defined with an interplanar distance of around 0.26 nm and 0.33 nm corresponding to planes (200) and (101), respectively, which are characteristic of SnO_2. Meanwhile, the SAED results (Fig. 4f) show a pattern of distinct dots and rings, indicating a highly crystalline character of the nanoparticles. In contrast, in the micrographs of SnO_2-blackberry and SnO_2-blueberry (Fig. 4g,j), a primarily amorphous character can be observed with a few isolated crystallographic planes with an interplanar distance of 0.33 nm corresponding to plane 101, the which is characteristic of SnO_2. However, for SnO_2-blueberry, we do not observe any crystallographic plane, this is attributed to the presence of the extract surrounding the SnO_2 nanoparticles, thus making it difficult to observe defined lattice fringes. The SAED results (Fig. 4i,l) show a diffuse ring pattern, which indicates an amorphous structure and is attributed to the presence of organic molecules that disrupt the alignment of [59] atoms. These results show

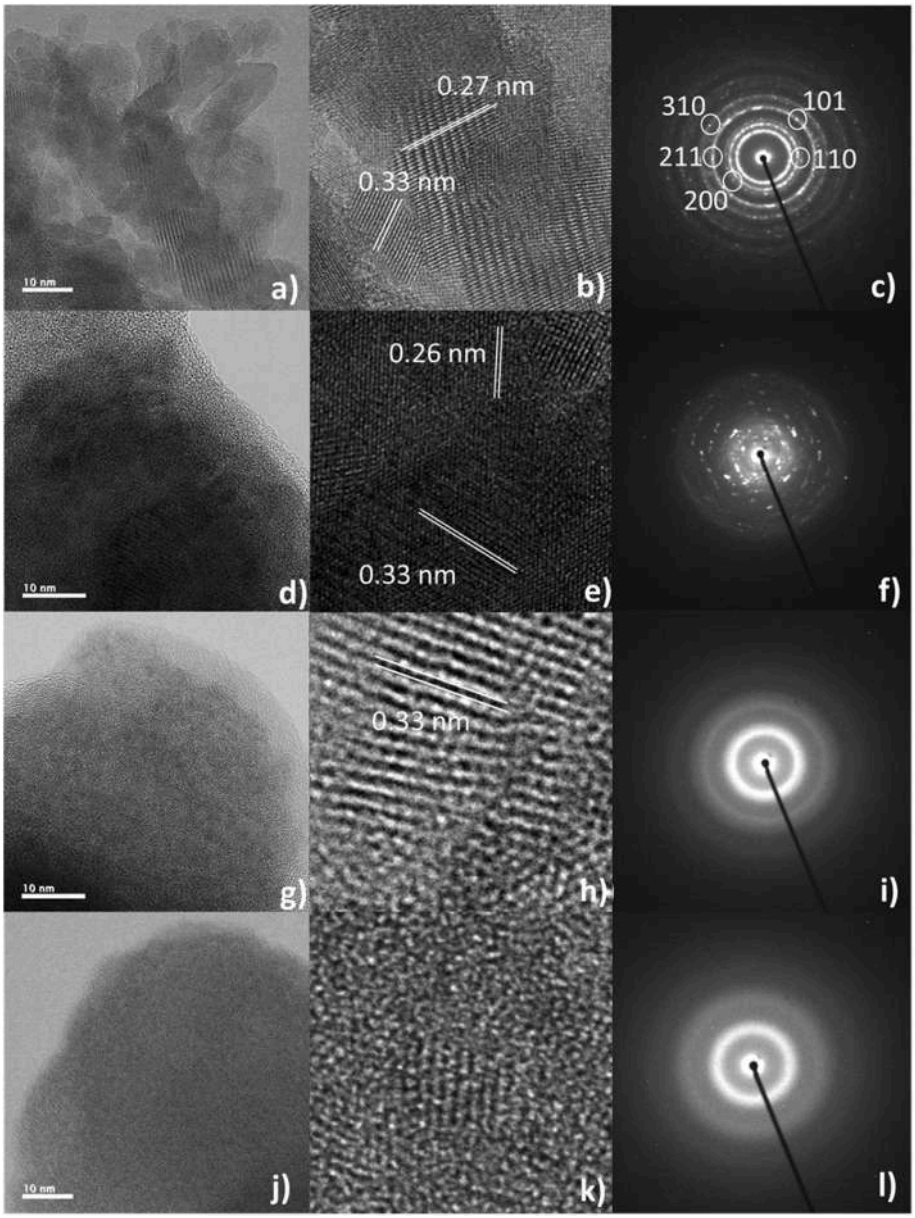

Fig. 4. HRTEM micrographs and SAED patterns of SnO_2 (a–c), SnO_2-beetroot (d–f) SnO_2-blackberry (g–i) and SnO_2-blueberry (j–l).

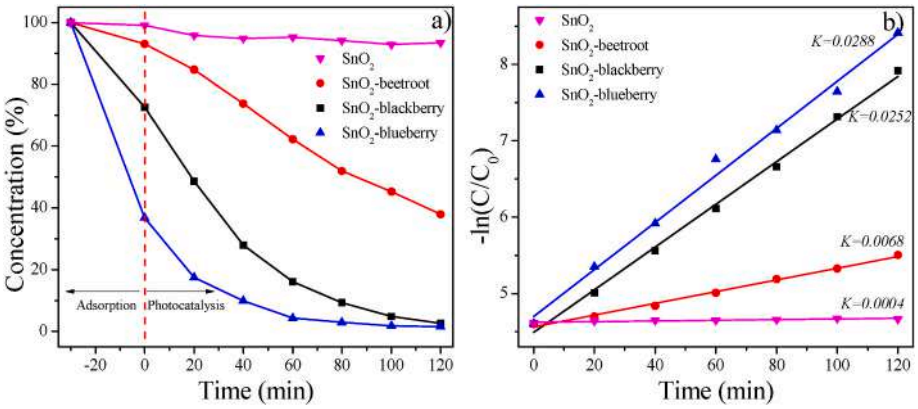

Fig. 5. Photocatalytic degradation of methylene blue (MB) under solar irradiation using the SnO_2 nanoparticles (a) and their degradation rate constants (b). (For interpretation of the references to color in this figure legend, the reader is referred to the Web version of this article.)

that the samples have a short-range polycrystalline character, which is interrupted by the presence of organic molecules in the extract, which are functionalized on the surface of the SnO_2 nanoparticles.

3.2. Photocatalytic activity

Fig. 5 shows the photocatalytic degradation and degradation rate constants (K) of SnO_2, SnO_2-blackberry, SnO_2-blueberry, and SnO_2-beetroot. Fig. 5a shows the photocatalytic degradation of methylene blue (MB) under solar irradiation. The SnO_2 nanoparticles did not present MB absorption before solar irradiation due to the SnO_2 surface not having any interaction with the MB molecules. After solar irradiation, pure SnO_2 showed a photocatalytic degradation of around 6.54% MB in 120 min. This is due to its bandgap value (3.0 eV) only allowing it to absorb ultraviolet light (~5%) and not the visible (~50%) portion of the solar spectrum [25]. It is worth mentioning that similar values have been previously reported for SnO_2 obtained by the hydrothermal method [60]. On the other hand, samples SnO_2-beetroot, SnO_2-blackberry, SnO_2-blueberry exhibited around 7%, 23%, and 62% MB absorption before solar irradiation, respectively, which were higher compared to pure SnO_2. This is attributed to the molecules of the extracts functionalized to the surface of the SnO_2 nanoparticles having good affinity with the cationic MB dye. After solar irradiation, the samples presented around 62%, 98%, and 100% of MB photocatalytic degradation, respectively, which shows better results than for SnO_2. The increase in the photocatalytic degradation of MB can be attributed to the extract acting as a photosensitizer for the SnO_2 nanoparticles, generating a decrease in the bandgap values for all the samples (see Fig. 2). This effect permits a broader absorption range of the sunlight spectrum for the SnO_2 nanoparticles (see the mechanism in Fig. 6).

In addition, Fig. 5b shows the calculations of the K values for the SnO_2, SnO_2-beetroot, SnO_2-blackberry, and SnO_2-blueberry samples, which were around 0.0004, 0.0068, 0.0252 and 0.0288, respectively. The SnO_2-blueberry sample showed a constant 72 times higher than that of pure SnO_2. This result can be attributed to the phenolic groups present in the blueberry pelargonidin showing an excellent affinity to binding to semiconductors [58]. Hence, a greater capacity to transfer electrons from the anthocyanins (natural dye) to the SnO_2 nanoparticles produces the best results of photocatalytic activity. In contrast, SnO_2-blackberry presented a constant 63 times higher than SnO_2 but lower than SnO_2--blueberry. This is because the blackberry anthocyanins have a lower affinity to bind to semiconductors, which generates a higher bandgap value [55]. Finally, the SnO_2-beetroot presented a constant 17 times higher than pure SnO_2 and lower than the previously mentioned samples. The outcome is attributed to its bandgap value being the highest (see Fig. 2), which would reduce the range of the visible light absorption and limit its application in sunlight [61].

3.3. Degradation mechanism

Fig. 6 shows the MB degradation mechanism for SnO_2 nanoparticles under solar irradiation. The improved performance of SnO_2 nanoparticles synthesized by this novel green method is mainly attributed to the extract before and during the photocatalytic process since it acts as (1) adsorbent and (2) photosensitizer.

(1) The excellent adsorption capacity of the extract is attributed to an electrostatic interaction that occurs between the extract molecules (negative charges) with the MB molecules (positive charges), which allows them to adsorb a higher concentration of MB onto the surface of the SnO_2 nanoparticles (see Fig. 6a). It is worth mentioning that this action has been reported as a requirement to allow the SnO_2 to increase its efficiency in the photocatalytic degradation of MB [5].
(2) When the SnO_2 nanoparticles with extract are irradiated under sunlight, two types of photocatalytic responses occur simultaneously. The first response is carried out in the semiconductor by ultraviolet light (~5% of sunlight), which causes the electrons to enter an excited state and move from the valence band (VB) to the conduction band (CB) of the semiconductor, generating a hole (h^+) in the VB and photogenerated electrons (e^-) in the CB (see Eq. (1)). It is worth mentioning that the generated electron-hole

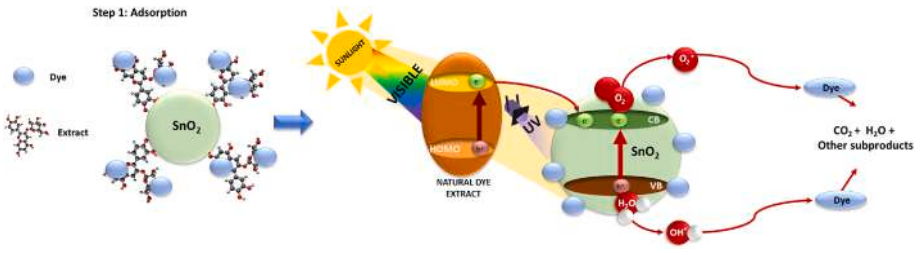

Fig. 6. Reaction mechanism of SnO_2 nanoparticles in the photocatalytic degradation of MB.

pair tend to recombine rapidly and only a small number of them (<1%) participate in the photocatalytic reaction. The second response is carried out in the extract by visible light (~50% of sunlight), which causes electrons to be excited from the highest occupied molecular orbital (HOMO) to the lowest unoccupied molecular orbital (LUMO) of the extract. Subsequently, the electrons found in the LUMO are injected into the CB of the semiconductor (see Eqs. (2) and (3)). The photogenerated electrons found in the CB photo-reduce the oxygen (O_2) diluted in the water, producing superoxide radicals ($O_2^{\bullet}$) (see Eq. (4)). Which are highly reactive and can form hydroxyl radicals ($OH^{\bullet}$) when interacting with H_2O (see Eq. (5)). Simultaneously, the holes (h^+) found in the VB photo-oxidize the H_2O molecules to produce more $OH^{\bullet}$ (see Eq. (6)). Finally, these radicals react with MB molecules producing non-toxic products such as H_2O, CO_2, and more species (see Eqs. (7) and (8)) [62]. The main reactions of the photocatalytic mechanism are summarized in the following equations:

$$SnO_2 + hv\ (UV) \rightarrow SnO_2\ (e^-_{CB}) + SnO_2\ (h^+_{VB}) \quad (1)$$

$$SnO_2/Dye + hv\ (Visible) \rightarrow SnO_2/Dye^* \quad (2)$$

$$SnO_2/Dye + hv\ (Visible) \rightarrow SnO_2/(Dye^+ + e^-_{CB}) \quad (3)$$

$$SnO_2(e^-_{CB}) + O_2 \rightarrow SnO_2/Dye + O_2^{\bullet} \quad (4)$$

$$O_2^{\bullet} + H_2O \rightarrow OH^{\bullet} \quad (5)$$

$$SnO_2\ (h^+_{VB}) + H_2O \rightarrow SnO_2 + OH^{\bullet} \quad (6)$$

$$OH^{\bullet} + MB_{adsorbed} \rightarrow H_2O + CO_2 + \text{Other products} \quad (7)$$

$$O_2^{\bullet} + MB_{adsorbed} \rightarrow H_2O + CO_2 + \text{Other products} \quad (8)$$

This mechanism describes the photocatalytic process of photosensitized SnO_2 nanoparticles under irradiation with sunlight, where an increase in the efficiency of MB degradation is shown. It is attributed to the fact that the extract acts as a photosensitizer allowing the semiconductor to be able to absorb the visible light during the photocatalytic process.

4. Conclusions

SnO_2 nanoparticles were successfully synthesized and photosensitized in one step using three different natural dye extracts through a novel and sustainable procedure. The characterization confirmed the synthesis and functionalization of the nanoparticles with the extracts. The presence of the natural dyes provoked a change in the bandgap of the nanoparticles, i.e., the value decreased from 3.0 to 2.7 eV for the pure and modified SnO_2, respectively. The experimental results showed that the natural dye extracts used in the synthesis significantly improved the solar photocatalytic activity of the nanoparticles when compared with pure SnO_2. In this sense, the photosensitized nanoparticles degraded up to 97.3% of an organic pollutant after 120 min of exposure to solar radiation. The results demonstrated that, with this new procedure, the synthesis and photosensitization of SnO_2, with good photocatalytic performance under solar radiation, can be carried out in a more efficient, simple, and sustainable manner.

Declaration of competing interest

The authors declare that they have no known competing financial interests or personal relationships that could have appeared to influence the work reported in this paper.

Acknowledgments

The authors thank DGIP-UAS PROFAPI 2022/PRO-A8-008 and CONACYT for their support in developing this work. Likewise, they wish to thank the technicians Karla Campos, Erika López, Adan Borunda, Mónica Mendoza, and Roberto Talamantes for their essential help in the laboratory.

References

[1] D.B. Walker, D.J. Baumgartner, C.P. Gerba, K. Fitzsimmons, Surface Water Pollution, third ed., Elsevier Inc., 2019.
[2] H. Qadri, R. Ahmad, B. Mohammad, A. Mehmood, G. Hamid, Fresh Water Pollution Dynamics and Remediation, Springer Singapore, Singapore, 2020.
[3] T. Hussain, A. Wahab, A critical review of the current water conservation practices in textile wet processing, J. Clean. Prod. 198 (2018) 806–819, https://doi.org/10.1016/j.jclepro.2018.07.051.
[4] G. Samchetshabam, A. Hussan, T.G. Choudhury, S. Gita, Impact of textile dyes waste on aquatic environments and its treatment, September, Environ. Ecol. 35 (2017) 2349–2353.
[5] H. Zangeneh, A.A.L. Zinatizadeh, M. Habibi, M. Akia, M. Hasnain Isa, Photocatalytic oxidation of organic dyes and pollutants in wastewater using different modified titanium dioxides: a comparative review, J. Ind. Eng. Chem. 26 (2015) 1–36, https://doi.org/10.1016/j.jiec.2014.10.043.
[6] D.S.M.I. Uddin, Impact of Textile Wastewater, November, Pakistan Text. J., 2018, pp. 38–39, https://doi.org/10.3844/ajessp.2007.
[7] L.S.R.R. Yadav, et al., Antibacterial and photocatalytic activities of ZnO nanoparticles: synthesized using water melon juice as fuel, Int. J. Nanosci. 15 (1–2) (2016) 1–8, https://doi.org/10.1142/S0219581X1650006X.
[8] M.U. Yousaf, E. Pervaiz, S. Minallah, M.J. Afzal, L. Honghong, M. Yang, Tin oxide quantum dots decorated graphitic carbon nitride for enhanced removal of organic components from water: green process, June, Results Phys. 14 (2019), 102455, https://doi.org/10.1016/j.rinp.2019.102455.
[9] B. Liu, Y. Fang, Z. Li, S. Xu, Visible-light nanostructured photocatalysts - a review, J. Nanosci. Nanotechnol. 15 (2) (2015) 889–920, https://doi.org/10.1166/jnn.2015.9784.
[10] S.N. Ahmed, W. Haider, Heterogeneous photocatalysis and its potential applications in water and wastewater treatment: a review, Nanotechnology 29 (34) (Aug. 2018), 342001, https://doi.org/10.1088/1361-6528/aac6ea.
[11] J.J. Rueda-Marquez, I. Levchuk, P. Fernández Ibañez, M. Sillanpää, A critical review on application of photocatalysis for toxicity reduction of real wastewaters, J. Clean. Prod. 258 (2020), https://doi.org/10.1016/j.jclepro.2020.120694.
[12] B. Zhu, C.M. Liu, M.B. Lv, X.R. Chen, J. Zhu, G.F. Ji, Structures, phase transition, elastic properties of SnO2 from first-principles analysis, Phys. B Condens. Matter 406 (18) (2011) 3508–3513, https://doi.org/10.1016/j.physb.2011.06.036.
[13] A. Diallo, E. Manikandan, V. Rajendran, M. Maaza, Physical & enhanced photocatalytic properties of green synthesized SnO2 nanoparticles via Aspalathus linearis, J. Alloys Compd. 681 (2016) 561–570, https://doi.org/10.1016/j.jallcom.2016.04.200.
[14] K. Kaviyarasu, et al., Photocatalytic activity of ZrO 2 doped lead dioxide nanocomposites: investigation of structural and optical microscopy of RhB organic dye, Appl. Surf. Sci. 421 (Nov. 2017) 234–239, https://doi.org/10.1016/j.apsusc.2016.11.149.
[15] J.W. Lee, R.H. Jeong, D.I. Kim, J.H. Yu, S.H. Nam, J.H. Boo, Facile synthesis of amorphous Ti-peroxo complex for photocatalytic activity under visible-light irradiation, J. Clean. Prod. 239 (2019), 118013, https://doi.org/10.1016/j.jclepro.2019.118013.
[16] B. Babu, A.N. Kadam, R.V.S.S.N. Ravikumar, C. Byon, Enhanced visible light photocatalytic activity of Cu-doped SnO2quantum dots by solution combustion synthesis, J. Alloys Compd. 703 (2017) 330–336, https://doi.org/10.1016/j.jallcom.2017.01.311.
[17] P. Amornpitoksuk, S. Suwanboon, S. Kaowphong, Photocatalytic activity of AgCl/SnO2 prepared by one-pot green synthesis, November, Sustain. Chem. Pharm. 14 (2019), 100190, https://doi.org/10.1016/j.scp.2019.100190.
[18] T. Yang, Q. Li, X. Chang, K.C. Chou, X. Hou, Preparation of TiOxNy/TiN composites for photocatalytic hydrogen evolution under visible light, Phys. Chem. Chem. Phys. 17 (43) (Oct. 2015) 28782–28788, https://doi.org/10.1039/C5CP04768D.
[19] Y. Zheng, et al., Electrostatic interaction assisted synthesis of a CdS/BCN heterostructure with enhanced photocatalytic effects, J. Mater. Chem. C 8 (5) (Feb. 2020) 1803–1810, https://doi.org/10.1039/C9TC05896F.
[20] Z. Fang, L. Zhang, T. Yang, L. Su, K.C. Chou, X. Hou, Cadmium sulfide with tunable morphologies: preparation and visible-light driven photocatalytic performance, Phys. E Low-dimensional Syst. Nanostructures 93 (Sep. 2017) 116–123, https://doi.org/10.1016/J.PHYSE.2017.06.003.
[21] K. Song, F. He, E. Zhou, L. Wang, H. Hou, W. Yang, Boosting solar water oxidation activity of BiVO4 photoanode through an efficient in-situ selective surface cation exchange strategy, J. Energy Chem. 68 (May 2022) 49–59, https://doi.org/10.1016/J.JECHEM.2021.11.024.
[22] K. Song, et al., Enhanced solar water splitting of BiVO4 photoanodes by in situ surface band edge modulation, J. Mater. Chem. 10 (42) (Nov. 2022) 22561–22570, https://doi.org/10.1039/D2TA06141D.
[23] B.N. Dimarco, R.N. Sampaio, E.M. James, T.J. Barr, M.T. Bennett, G.J. Meyer, Efficiency considerations for SnO2-based dye-sensitized solar cells, ACS Appl. Mater. Interfaces 12 (21) (2020) 23923–23930, https://doi.org/10.1021/acsami.0c04117.

[24] M.R. Narayan, Review: dye sensitized solar cells based on natural photosensitizers, Renew. Sustain. Energy Rev. 16 (1) (2012) 208–215, https://doi.org/10.1016/j.rser.2011.07.148.
[25] S. Goulart, L.J. Jaramillo Nieves, A.G. Dal Bó, A.M. Bernardin, Sensitization of TiO2 nanoparticles with natural dyes extracts for photocatalytic activity under visible light, February, Dyes Pigments 182 (2020), 108654, https://doi.org/10.1016/j.dyepig.2020.108654.
[26] C. Diaz-Uribe, et al., Potential use of an anthocyanin-rich extract from berries of Vaccinium meridionale Swartz as sensitizer for TiO2 thin films – an experimental and theoretical study, May, J. Photochem. Photobiol. Chem. 384 (2019), 112050, https://doi.org/10.1016/j.jphotochem.2019.112050.
[27] G. Richhariya, A. Kumar, P. Tekasakul, B. Gupta, Natural dyes for dye sensitized solar cell: a review, April 2015, Renew. Sustain. Energy Rev. 69 (2017) 705–718, https://doi.org/10.1016/j.rser.2016.11.198.
[28] M. Shahid, Shahid-ul-Islam, F. Mohammad, Recent advancements in natural dye applications: a review, J. Clean. Prod. 53 (Aug. 2013) 310–331, https://doi.org/10.1016/j.jclepro.2013.03.031.
[29] A. Bartolotta, G. Calogero, Dye-sensitized Solar Cells: from Synthetic Dyes to Natural Pigments, Elsevier Ltd, 2019.
[30] N.A. Ludin, A.M. Al-Alwani Mahmoud, A. Bakar Mohamad, A.A.H. Kadhum, K. Sopian, N.S. Abdul Karim, Review on the development of natural dye photosensitizer for dye-sensitized solar cells, Renew. Sustain. Energy Rev. 31 (2014) 386–396, https://doi.org/10.1016/j.rser.2013.12.001.
[31] S. Hao, J. Wu, Y. Huang, J. Lin, Natural dyes as photosensitizers for dye-sensitized solar cell, Sol. Energy 80 (2) (Feb. 2006) 209–214, https://doi.org/10.1016/j.solener.2005.05.009.
[32] K. Wongcharee, V. Meeyoo, S. Chavadej, Dye-sensitized solar cell using natural dyes extracted from rosella and blue pea flowers, Sol. Energy Mater. Sol. Cells 91 (7) (Apr. 2007) 566–571, https://doi.org/10.1016/j.solmat.2006.11.005.
[33] F. Zanjanchi, J. Beheshtian, Natural pigments in dye-sensitized solar cell (DSSC): a DFT-TDDFT study, J. Iran. Chem. Soc. 16 (4) (2019) 795–805, https://doi.org/10.1007/s13738-018-1561-2.
[34] D. Vásquez, F. Palominos, S. Martínez, Visible-light photocatalytic degradation of aniline blue by stainless-steel foam coated with TiO2 grafted with anthocyanins from a Maqui-blackberry system, Catalysts 10 (11) (Oct. 2020) 1245, https://doi.org/10.3390/catal10111245.
[35] Z. Yan, et al., Visible-light degradation of dyes and phenols over mesoporous titania prepared by using anthocyanin from red radish as template, 2014, Int. J. Photoenergy (2014), https://doi.org/10.1155/2014/968298.
[36] E. Gomathi, K. Kumaraguru, Green synthesis and photogenerated charge carriers transfer in SnO2 QDs decorated rGO nanosheets for highly efficient visible light photocatalysis, J. Inorg. Organomet. Polym. Mater. 28 (4) (2018) 1664–1670, https://doi.org/10.1007/s10904-018-0844-5.
[37] B. Kumar, K. Smita, L. Cumbal, A. Debut, Y. Angulo, Biofabrication of copper oxide nanoparticles using Andean blackberry (Rubus glaucus Benth.) fruit and leaf, J. Saudi Chem. Soc. 21 (2017) S475–S480, https://doi.org/10.1016/j.jscs.2015.01.009.
[38] K.S. Vizuete, B. Kumar, A.V. Vaca, A. Debut, L. Cumbal, Mortiño (Vaccinium floribundum Kunth) berry assisted green synthesis and photocatalytic performance of Silver–Graphene nanocomposite, J. Photochem. Photobiol. Chem. 329 (2016) 273–279, https://doi.org/10.1016/j.jphotochem.2016.06.030.
[39] M.A. Pavan Kumar, D. Suresh, H. Nagabhushana, S.C. Sharma, Beta vulgaris aided green synthesis of ZnO nanoparticles and their luminescence, photocatalytic and antioxidant properties, Eur. Phys. J. Plus 130 (6) (2015), https://doi.org/10.1140/epjp/i2015-15109-2.
[40] N. Matinise, X.G. Fuku, K. Kaviyarasu, N. Mayedwa, M. Maaza, ZnO nanoparticles via Moringa oleifera green synthesis: physical properties & mechanism of formation, Appl. Surf. Sci. 406 (Jun. 2017) 339–347, https://doi.org/10.1016/j.apsusc.2017.01.219.
[41] A. Faria, et al., Antioxidant properties of prepared blueberry (Vaccinium myrtillus) extracts, J. Agric. Food Chem. 53 (17) (2005) 6896–6902, https://doi.org/10.1021/jf0511300.
[42] C. Mertz, V. Cheynier, Z. Günata, P. Brat, Analysis of phenolic compounds in two blackberry species (Rubus glaucus and Rubus adenotrichus) by high-performance liquid chromatography with diode array detection and electrospray ion trap Mass spectrometry, J. Agric. Food Chem. 55 (21) (Oct. 2007) 8616–8624, https://doi.org/10.1021/jf071475d.
[43] J. Leyrer, M. Rubilar, E. Morales, B. Pavez, E. Leal, R. Hunter, Factor optimization in the manufacturing process of dye-sensitized solar cells based on naturally extracted dye from a Maqui and blackberry mixture (aristotelia chilensis and Rubus glaucus), J. Electron. Mater. 47 (10) (2018) 6136–6143, https://doi.org/10.1007/s11664-018-6514-0.
[44] A.R. Hernández-Martínez, M. Estévez, S. Vargas, R. Rodríguez, Stabilized conversion efficiency and Dye-Sensitized solar cells from Beta vulgaris pigment, Int. J. Mol. Sci. 14 (2) (2013) 4081–4093, https://doi.org/10.3390/ijms14024081.
[45] H. Zhou, L. Wu, Y. Gao, T. Ma, Dye-sensitized solar cells using 20 natural dyes as sensitizers, J. Photochem. Photobiol. Chem. 219 (2–3) (2011) 188–194, https://doi.org/10.1016/j.jphotochem.2011.02.008.
[46] K. Manquián-Cerda, E. Cruces, M. Angélica Rubio, C. Reyes, N. Arancibia-Miranda, Preparation of nanoscale iron (oxide, oxyhydroxides and zero-valent) particles derived from blueberries: reactivity, characterization and removal mechanism of arsenate, November, Ecotoxicol. Environ. Saf. 145 (2017) 69–77, https://doi.org/10.1016/j.ecoenv.2017.07.004.
[47] P.A. Luque, et al., Improved photocatalytic efficiency of SnO2 nanoparticles through green synthesis, January, Optik 206 (2020), https://doi.org/10.1016/j.ijleo.2020.164299.
[48] M. Honarmand, M. Golmohammadi, A. Naeimi, Green synthesis of SnO2-bentonite nanocomposites for the efficient photodegradation of methylene blue and eriochrome black-T, Mater. Chem. Phys. 241 (Feb. 2020), 122416, https://doi.org/10.1016/j.matchemphys.2019.122416.
[49] B. Troudi, et al., Eco-friendly synthesis of metal oxide nanoparticles using carissa, Mater. Sci. Semicond. Process. 5 (2) (2016) 88–96, https://doi.org/10.20959/wjpr20167-6472.
[50] S.N. Matussin, M.H. Harunsani, A.L. Tan, A. Mohammad, M.H. Cho, M.M. Khan, Photoantioxidant studies of SnO2 nanoparticles fabricated using aqueous leaf extract of Tradescantia spathacea, April, Solid State Sci. 105 (2020), 106279, https://doi.org/10.1016/j.solidstatesciences.2020.106279.
[51] S. Kundu, A. Kumar, S. Sen, A. Nilabh, Bio-synthesis of SnO2 and comparison its CO sensing performance with conventional processes, J. Alloys Compd. 818 (2020), 152841, https://doi.org/10.1016/j.jallcom.2019.152841.
[52] D.B. Jadhav, R.D. Kokate, Green synthesis of SnO2 using green papaya leaves for nanoelectronics (LPG sensing) application, Mater. Today Proc. 26 (xxxx) (2019) 998–1004, https://doi.org/10.1016/j.matpr.2020.01.180.
[53] F. Puga, J.A. Navío, M.C. Hidalgo, Enhanced UV and visible light photocatalytic properties of synthesized AgBr/SnO2 composites, Separ. Purif. Technol. 257 (2021), 117948, https://doi.org/10.1016/j.seppur.2020.117948.
[54] A. Lim, P. Ekanayake, L.B.L. Lim, J.M.R.S. Bandara, Co-dominant effect of selected natural dye sensitizers in DSSC performance, Spectrochim. Acta Part A Mol. Biomol. Spectrosc. 167 (2016) 26–31, https://doi.org/10.1016/j.saa.2016.05.024.
[55] M. Ghosh, P. Chowdhury, A.K. Ray, Photocatalytic activity of aeroxide tio2 sensitized by natural dye extracted from mangosteen peel, Catalysts 10 (8) (2020), https://doi.org/10.3390/catal10080917.
[56] M. Megala, J. Mayandi, B.J.M. Rajkumar, Optical absorption study of anthoxanthin based natural dyes for dye sensitized solar cells: experimental and theoretical investigations, Mater. Lett. 276 (2020), 128089, https://doi.org/10.1016/j.matlet.2020.128089.
[57] R. Sha, S. Badhulika, Facile green synthesis of reduced graphene oxide/tin oxide composite for highly selective and ultra-sensitive detection of ascorbic acid, March, J. Electroanal. Chem. 816 (May 2018) 30–37, https://doi.org/10.1016/j.jelechem.2018.03.033.
[58] F. Teoli, et al., Role of pH and pigment concentration for natural dye-sensitized solar cells treated with anthocyanin extracts of common fruits, J. Photochem. Photobiol. Chem. 316 (2016) 24–30, https://doi.org/10.1016/j.jphotochem.2015.10.009.
[59] S. Begum, M. Ahmaruzzaman, Green synthesis of SnO2 quantum dots using Parkia speciosa Hassk pods extract for the evaluation of anti-oxidant and photocatalytic properties, J. Photochem. Photobiol. B Biol. 184 (2018) 44–53, https://doi.org/10.1016/j.jphotobiol.2018.04.041.
[60] A. Mamakhel, M. Søndergaard, K. Borup, B. Brummerstedt Iversen, Continuous flow hydrothermal synthesis of rutile SnO2 nanoparticles: exploration of pH and temperature effects, J. Supercrit. Fluids 166 (2020) 1–8, https://doi.org/10.1016/j.supflu.2020.105029.
[61] C. Diaz-Uribe, et al., TiO2 thin films sensitization with natural dyes extracted from Bactris guineensis for photocatalytic applications: experimental and DFT study, J. Saudi Chem. Soc. 24 (5) (2020) 407–416, https://doi.org/10.1016/j.jscs.2020.03.004.
[62] S. Krishnan, A. Shriwastav, Application of TiO2 nanoparticles sensitized with natural chlorophyll pigments as catalyst for visible light photocatalytic degradation of methylene blue, J. Environ. Chem. Eng. 9 (1) (2021), 104699, https://doi.org/10.1016/j.jece.2020.104699.